Orientation of Polymer Coils in Dilute Solutions Undergoing Shear Flow: Birefringence and Light Scattering

Jacques Bossart* and Hans Christian Öttinger

Institut für Polymere, Eidgenössische Technische Hochschule Zürich, ETH-Zentrum, CH-8092 Zürich, Switzerland

Received March 9, 1995; Revised Manuscript Received June 1, 1995®

ABSTRACT: Polymer orientation can be investigated on different length scales by means of various measurement techniques such as flow birefringence or light scattering. We start from equations that relate the orientation angle of polymers to the tensorial quantities measured by experimental means. A quantity called "orientation resistance" of the polymer coils is introduced for the mentioned techniques and for translational diffusion. We calculate the orientation resistance for dilute Θ solutions undergoing shear flow in the framework of bead–spring models including hydrodynamic interaction by various approximation schemes. We show that the results of the Gaussian approximation, as well as the perturbation theory, differ considerably from the simple Rouse and Zimm results. In order to make a comparison to flow birefringence and light scattering experiments as meaningful as possible, we carefully study the polydispersity effect on the orientation angle measurements for Θ and good solvents. It turns out that the predictions for the orientation angle are very sensitive to polydispersity and that in the limit of vanishing shear rate this effect can be handled in a simple way. A comparison to experiments from the literature suggests that orientation angle measurements could be used to determine the polydispersity of a polymer system in dilute solutions.

1. Introduction

On the one hand, kinetic theory models were developed primarily with the intention of making predictions about rheological quantities such as viscosity or normal stress differences. On the other hand, rheological properties of flowing polymer solutions are governed by the deformability and the orientational behavior, i.e., by the microstructural changes of the macromolecules, which can be investigated experimentally by flow birefringence[1–6] and scattering methods.[7–9] If such measurements are compared to theoretical calculations of quantities such as the orientation angle of polymer coils, they constitute further tests of kinetic theory model predictions.

Since it is important to have knowledge about the anisotropy of the polymer coils on different length scales, we will also investigate the orientational behavior arising from the translational diffusion properties of the macromolecules.

Considering dilute polymer solutions undergoing simple shear flow, we want to emphasize in the next section that the orientation angles measured by flow birefringence and by light scattering experiments cannot be directly compared. We explicitly show in the framework of kinetic models that flow birefringence and light scattering lead to different results. The reason for this discrepancy lies in the fact that flow birefringence corresponds to an averaging of the stress tensor whereas light scattering for small scattering vectors is identified with the gyration tensor. In both cases it is possible to write down an equation that relates the orientation angle to the components of the corresponding tensor (section 2).

In section 3, we calculate both tensors for Θ solutions by means of bead–spring models.[10] The rheological properties of dilute polymer solutions are affected by the phenomenon of hydrodynamic interaction (non-free-draining coils). Therefore, the analytically solvable Rouse model[11] has to be modified to account for hydrodynamic interaction effects. Since we want to perform our calculations analytically, we will make use of different approximation schemes (Zimm,[12] Gaussian approximation,[13,14] and renormalization group refinement of perturbation series results.[15]

In section 4, we show how polydispersity corrections have to be performed in order to compare different experimental results and experiments to theory. Since it turns out that the measurement of the orientation resistance is very sensitive to polydispersity and to the type of molar mass distribution, we suggest using it as a method to determine the polydispersity of a dilute polymer solution.

2. Flow Birefringence and Light Scattering

The flow birefringence of polymer solutions has two origins: form birefringence arising from the anisotropy in the correlation of the segment density and intrinsic birefringence coming from the orientation of polymer segments. For the latter there exists the so-called stress-optical law. It relates the components of the stress tensor to the optical properties of the flowing fluid.

In the case of a simple shear flow, the form of the stress tensor is given by[10]

$$\boldsymbol{\tau} = \begin{bmatrix} \tau_{11} & \tau_{12} & 0 \\ \tau_{21} & \tau_{22} & 0 \\ 0 & 0 & \tau_{33} \end{bmatrix} \quad \text{and } \tau_{12} = \tau_{21} \qquad (1)$$

in the orthogonal laboratory system, where the direction (1) is that of the streamlines and the direction (2) is that of the velocity gradient. The plane (1,2) is the plane of flow, and the direction (3) is normal to this plane.

The geometrical representation of this tensor is an ellipsoid called the stress ellipsoid. The orientation angle χ_τ of this ellipsoid is given by the angle between the direction (1) and the major axis of the stress ellipsoid. The transformation law for the stress tensor from the laboratory system to the principal axes of the stress ellipsoid is given by

® Abstract published in *Advance ACS Abstracts,* July 15, 1995.

0024-9297/95/2228-5852$09.00/0

$$\tan 2\chi_\tau = \frac{2\tau_{21}}{\tau_{11} - \tau_{22}} =: \frac{m_\tau(\beta)}{\beta} \tag{2}$$

where the dimensionless quantity β is the reduced shear rate

$$\beta := \frac{[\eta]_0 \eta_s M}{RT}\dot{\gamma}, \qquad [\eta]_0 := \lim_{\dot{\gamma}\to 0}\lim_{c_p\to 0}\frac{\eta_p}{c_p\eta_s} \tag{3}$$

($\dot{\gamma}$ = time-independent shear rate, c_p = polymer concentration, $[\eta]_0$ = zero-shear-rate intrinsic viscosity, η_s = solvent viscosity, M = molecular weight, R = universal gas constant, T = absolute temperature). The quantity $[\eta]_0\eta_s M/RT$ is a characteristic time constant for the polymer solution suggested by molecular theories.[10]

The stress optical law states that the corresponding orientation angle χ of the index ellipsoid coincides with the angle χ_τ,

$$\chi = \chi_\tau \tag{4}$$

The angle χ_τ can therefore be interpreted as the orientation angle of the macromolecule measured by flow birefringence.

The second part of eq 2 should be understood as a definition of the quantity $m_\tau(\beta)$. The motivation to write the above ratio of the stress tensor components as a dimensionless function $m_\tau(\beta)$ divided through the reduced shear rate β is related to the fact that for small shear rates the shear stress τ_{21} increases linearly and the first normal stress difference increases quadratically with reduced shear rate β.[10,13,15] The function $m_\tau(\beta)$ therefore tends to an intrinsic nonvanishing value m_τ^0 for the zero-shear-rate limit ($\beta \to 0$).

In linear viscoelastic models the inverse of the quantity m_τ^0 is called the reduced steady-state compliance.[1,16] For a dilute polymer solution we will therefore call $m_\tau(\beta)$ the "orientation resistance". This expression has already been suggested in ref 9.

Let us now turn to static light scattering experiments, where the time-averaged intensity of the scattered light is measured. For dilute solutions, the concentration c_p of the polymers is assumed to be much smaller than the overlap concentration. Therefore, the intermolecular structure factor can be neglected since no interaction between the individual polymers occurs. Then, the light intensity scattered by the macromolecules or the experimentally accessible Rayleigh ratio (see, e.g., ref 18) can be related to the form factor $P(\mathbf{q})$[17,18]

$$P(\mathbf{q}) = \frac{1}{N^2}\left\langle \sum_{j,k=1}^{N} \exp[i\mathbf{q}\cdot\mathbf{r}_{jk}]\right\rangle \tag{5}$$

$$\mathbf{r}_{jk} := \mathbf{r}_j - \mathbf{r}_k \tag{6}$$

where $\mathbf{r}_{jk}$ denotes the difference vector between the individual scattering units of the polymer, N is the number of scattering units, and $\mathbf{q}$ is the scattering vector with

$$|\mathbf{q}| = \frac{4\pi n_0}{\lambda_0}\sin\frac{\theta}{2} \qquad (\theta = \text{scattering angle}) \tag{7}$$

In eq 5 $\langle ... \rangle$ represents the average over all possible configurations of the difference vector $\mathbf{r}_{jk}$. The refractive index of the solvent medium is denoted by n_0 and the wavelength in the solvent by λ_0, respectively.

Unfortunately, not even in the Rouse model can the form factor (5) be calculated in a closed form,[19,20] so that $P(\mathbf{q})$ must be evaluated in the so-called Guinier regime in order to interpret experimental data. This regime is obtained for

$$|\mathbf{q}|\langle R_G^2\rangle^{1/2} \ll 1 \tag{8}$$

By $\langle R_G^2\rangle$ we denote the mean-square radius of gyration. Thus, assuming that the distribution of the vectors $\mathbf{r}_{jk}$ is isotropic, the first order in the series expansion of the exponential in eq 5 is vanishing and, if we neglect terms that are of higher than second order in the series expansion, the form factor can be written as

$$P(\mathbf{q}) = 1 - \mathbf{q}\cdot\mathbf{G}\cdot\mathbf{q} \tag{9}$$

where $\mathbf{G}$ is the gyration tensor,

$$\mathbf{G} := \frac{1}{2N^2}\sum_{j,k=1}^{N}\langle \mathbf{r}_{jk}\mathbf{r}_{jk}\rangle \tag{10}$$

$$= \frac{1}{N}\sum_{j=1}^{N}\langle (\mathbf{r}_j - \mathbf{r}_c)(\mathbf{r}_j - \mathbf{r}_c)\rangle \tag{11}$$

In eq 11, $\mathbf{r}_c$ means the position vector of the center of mass of the polymer. Note that the term $\mathbf{q}\cdot\mathbf{G}\cdot\mathbf{q}$ involves the projection of the gyration tensor on the direction of the scattering vector $\mathbf{q}$.

We want to make two comments on eq 9: First, in this approximation the gyration tensor is the only quantity determining the form factor. Therefore, the molecular orientation measured by light scattering is given by the orientation of the gyration ellipsoid. Second, the form factor, and thus the intensity of the scattered light, have a minimum when the direction of the scattering vector coincides with the major axis of the ellipsoid belonging to the gyration tensor. Thus, the orientation angle can be determined by variation of the scattering vector orientation.[7,8,21]

Thus we write down an equation similar to eq 2

$$\tan 2\chi_G = \frac{2G_{21}}{G_{11} - G_{22}} =: \frac{m_G(\beta)}{\beta} \tag{12}$$

where χ_G is the orientation angle of the macromolecules measured by static light scattering and $m_G(\beta)$ is the corresponding orientation resistance.

A priori there is no reason why the orientation resistance m_τ measured by flow birefringence experiments should coincide with the orientation resistance m_G measured by light scattering experiments. Kröger et al.[22] showed in a nonequilibrium molecular dynamics (NEMD) simulation for polymer melts undergoing shear flow that the static structure factor, and hence the orientation angle of the polymer ellipsoid, depends on the value of the scattering vector $|\mathbf{q}|$. In agreement with small-angle neutron scattering (SANS) results,[23,24] they found a decreasing of $\pi/2 - \chi$ with increasing $|\mathbf{q}|$; i.e., the more local the dynamics is, the more pronounced the resistance against orientation becomes. Particularly, it has been shown in ref 24 that the extinction angle from flow birefringence coincides with the polymer orientation angle determined by SANS at a more local scale ($|\mathbf{q}| \simeq 4 \times 10^{-2}$ Å^{-1}) than the one given by the

radius of gyration. Indeed we will show in the next section that the corresponding theoretical value m_τ in dilute solutions is larger than m_G and m_D, where m_D denotes the orientation resistance for the diffusion tensor.

3. Orientation Resistance in Bead–Spring Models

In bead–spring models, polymers are modeled by chains consisting of N identical beads connected by $(N-1)$ springs. The velocity field $\mathbf{v}(\mathbf{r})$ of the incompressible Newtonian solvent is assumed to be homogeneous, i.e., of the form $\mathbf{v}(\mathbf{r}) = \mathbf{v}_0 + \kappa(t)\cdot\mathbf{r}$ with a constant vector $\mathbf{v}_0$ and a traceless second-rank tensor $\kappa(t)$ independent of the position $\mathbf{r}$. Here we consider Hookean springs, include hydrodynamic interaction by means of the Oseen–Burger tensor, but neglect excluded volume effects. Renormalization group calculations suggest that m_τ is only slightly affected by the excluded volume effect:[25] the improvement of the solvent quality slightly lowers the orientation resistance. It has also been shown experimentally by flow birefringence[1,26] that the excluded volume effect has practically no influence on the reduced steady-state compliance, which is the inverse of the orientation resistance m_τ. Furthermore, we will explain in this section why the orientation resistance m_D arising from the diffusion tensor is not altered by the excluded volume effect in first-order perturbation theory.

While both the neglect (Rouse model) and the preaveraging of hydrodynamic interaction (Zimm model) lead to Gaussian-distributed connector vectors, the fluctuations in the hydrodynamic interaction are highly nonlinear effects. These have been treated by the so-called Gaussian approximation[13,14] and by perturbation theory.[15]

Instead of the diffusion equation for the distribution function, time evolution equations for the second moments of the bead connector vectors, $\langle \mathbf{Q}_j\mathbf{Q}_k\rangle$, can be derived. They are the starting point for calculations performed in bead–spring models.[13] The stress tensor $\boldsymbol{\tau}^p$, the gyration tensor $\mathbf{G}$, and the translational diffusion tensor $\mathbf{D}$ can be written in the following way[10]

$$\boldsymbol{\tau}^p = -n_p H \sum_{j=1}^{N-1} \langle \mathbf{Q}_j\mathbf{Q}_j\rangle + (N-1)nkT\boldsymbol{\delta} \tag{13}$$

$$\mathbf{G} = \frac{1}{N}\sum_{j=1}^{N} \langle (\mathbf{r}_j - \mathbf{r}_c)(\mathbf{r}_j - \mathbf{r}_c)\rangle = \frac{1}{N}\sum_{j,k=1}^{N-1} C_{jk}\langle \mathbf{Q}_j\mathbf{Q}_k\rangle \tag{14}$$

$$\mathbf{D} = \frac{k_B T}{\zeta N}\left(\boldsymbol{\delta} + \frac{\zeta}{N}\sum_{\substack{j,k=1\\ j\neq k}}^{N} \langle \boldsymbol{\Omega}_{jk}\rangle\right) \tag{15}$$

Here C_{jk} denotes the Kramers matrix,[10] which is the inverse of the Rouse matrix and the Oseen–Burger tensor[10] which describes a long-range interaction and is denoted by $\boldsymbol{\Omega}_{ij} := \boldsymbol{\Omega}(\mathbf{r}_j - \mathbf{r}_k)$. The quantity n_p in eq 13 means the number density of polymers, ζ is the bead friction coefficient, H denotes the spring constant, and k_B is the Boltzmann constant. Note that eq 15 is only an approximate expression for the diffusion tensor.

Next we discuss the orientation resistance m for the different tensors calculated in the framework of different approximation schemes for the time evolution equations for the second moments $\langle \mathbf{Q}_j\mathbf{Q}_k\rangle$.

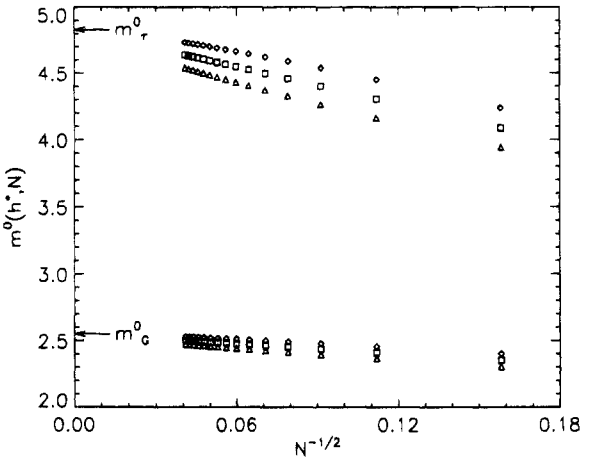

Figure 1. Intrinsic orientation resistance predicted by the Zimm model for the stress and the gyration tensor vs $N^{-1/2}$ for $h^* = 0.2218$ (△), $h^* = 0.2418$ (□), and $h^* = 0.2618$ (◇). The arrows indicate the limiting values of the curves for $N \to \infty$.

3.1. Rouse and Zimm Model. We consider the Rouse model[11] (no hydrodynamic interaction) for a simple shear flow characterized by the velocity gradient tensor κ for shear flow

$$\kappa = \dot\gamma \begin{bmatrix} 0 & 1 & 0 \\ 0 & 0 & 0 \\ 0 & 0 & 0 \end{bmatrix} \tag{16}$$

The stress (13) and the gyration tensor (14) can be calculated from the explicitly known solution of the time evolution equations for the second moments (see, e.g., ref 15). Equations 2 and 12 in the infinite chain limit then lead to

$$m^0_\tau = \lim_{N\to\infty} \frac{N^2}{6}\frac{\mathrm{Tr}(C)}{\mathrm{Tr}(C^2)} = \frac{5}{2} \qquad m^0_G = \lim_{N\to\infty} \frac{N^2}{6}\frac{\mathrm{Tr}(C^2)}{\mathrm{Tr}(C^3)} = \frac{7}{4} \tag{17}$$

In the case of the Zimm model (hydrodynamic interaction in a preaveraged form), the Kramers matrix (C_{jk}) in the expression for the orientation resistance m^0_τ has to be replaced by the inverse of the modified Rouse matrix, $(\check{C}_{jk})$,[10] which is not known analytically. However, its trace, $\mathrm{Tr}(\check{C})$, is analytically known in a closed form and $\mathrm{Tr}(\check{C}^2)$ can be evaluated from a series expansion with very high precision.[28] Therefore, m^0_τ can be calculated exactly in the limit $N \to \infty$, where the result does not depend any more on a specific value for the dimensionless hydrodynamic interaction parameter $h^* := (\zeta/\eta_s)(H/36\pi^3 k_B T)^{1/2}$. This parameter measures the strength of the hydrodynamic interaction. The obtained value is $m^0_\tau = 4.832496061$. We emphasize that the matrix $(\check{C}_{jk})$ depends on h^*. The traces $\mathrm{Tr}(C\check{C})$ and $\mathrm{Tr}(C\check{C}^2)$ which are necessary for the calculation of m^0_G must be found numerically and thus the calculation of the orientation resistance m^0_G depends on the value of h^* and N. For illustration, we display in Figure 1 the orientation resistance not only for the gyration tensor but also for the stress tensor for various values of the hydrodynamic interaction parameter h^* (0.2218, 0.2418, 0.2618) and N (40, 80, ..., 600). For $h^* = 0$ one recovers the Rouse values. Whereas an upper limit of the hydrodynamic interaction parameter can be estimated in the Zimm model[10] ($h^* \le 0.5$), renormalization group considerations lead to the value $h^* = 0.18$, which is a fixed point value characterizing the long-chain behavior.

Table 1. Orientation Resistance for the Stress, the Gyration, and the Diffusion Tensors in the Rouse and the Zimm Models, the Gaussian Approximation, and the First-Order Perturbation Theory Refined by the Renormalization Group Method (RG)

m	Rouse	Zimm	Gauss	RG
m_τ^0	2.50	4.832	3.57(2)	3.28
m_G^0	1.75	2.553(3)	2.00(2)	1.70
m_D^0	*	*	2.00(2)	1.98

From fitting experimental data to the Zimm theory, a range of 0.1...0.25 for h^* is obtained.[27] Within the range of reasonable h^* values, the best convergence (when $N \to \infty$) for m_τ^0 and m_G^0 is obtained at the value $h^* = 0.2418$; however, a careful extrapolation of the data in Figure 1 confirms that for $h^* > 0$ the values m_τ^0 and m_G^0 are independent of h^* in the limit of infinitely long chains. In Figure 1, m_τ and m_G are plotted vs $N^{-1/2}$ because, for the Zimm model, the leading corrections to the limit of infinitely long chains are of the order $N^{-1/2}$.[28] From a linear regression analysis of orders 5 through 13 in $N^{-1/2}$, we obtain the extrapolated values displayed in Table 1. We note, however, that a linear regression should be used for the statistical analysis of data with error bars whereas our orientation resistance data for each fixed N are exact. Nevertheless, the Zimm value of m_τ^0 obtained with this procedure (for $N \to \infty$) coincides very well with the above-mentioned exact calculation based on the traces $\mathrm{Tr}(\check{C})$ and $\mathrm{Tr}(\check{C}^2)$ in the limit $N \to \infty$ ($m_\tau^0 = 4.832496061$). Therefore, we generally use linear regression for the extrapolation of our orientation resistance values. At this point we would like to emphasize that our m_τ^0 value obtained in the Zimm model is slightly lower than the one given by Zimm in ref 12, namely, $m_\tau^0 = 4.88$. In the eigenvalue problem occurring in the solution procedure for the second moments in the Zimm model, the eigenvalues must be calculated numerically. In ref 29, Zimm calculated the higher eigenvalues by means of an asymptotic formula. The numerical procedure is the reason for this small discrepancy.

The diffusion tensor in the Rouse, as well as in the Zimm model, is isotropic.[10] Therefore, it is not possible in these models to assign an orientation resistance to the diffusion tensor.

From this investigation we see that for the Rouse as well as for the Zimm model the values for the orientation resistance are independent of the shear rate. Experiments, however, show a slight shear-rate dependence.[1,8,9] Therefore, we want to include fluctuations in hydrodynamic interaction by using the Gaussian approximation and perturbation theory.

3.2. Gaussian Approximation. With the assumption of a Gaussian distribution function, the higher moments occurring in the time evolution equations for the second moments can be reduced to expressions containing only three-dimensional integrals.[13] The integration procedure involves the evaluation of elliptic integrals for each time t so that the shear-rate-dependent solution can only be obtained numerically. On the other hand, if we restrict ourselves to small shear rates, there exists an analytical expression for the second moments $\langle \mathbf{Q}_j \mathbf{Q}_k \rangle$ and therefore for the intrinsic (zero-shear-rate) orientation resistance. The calculation involves the inversion of an $(N-1)^2 \times (N-1)^2$ matrix, whereas for the Zimm model the $(N-1) \times (N-1)$ modified Rouse matrix has to be inverted. Therefore, the extrapolation has been performed similarly to the procedure described above, but with smaller values of N (6...29). The resulting values for the intrinsic orientation resistance are displayed in Table 1.

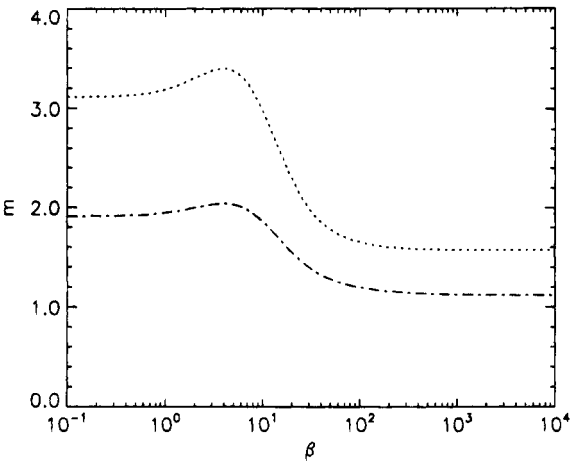

Figure 2. Orientation resistance m_τ (- - -) and m_G (— - —): Gaussian approximation for shear-dependent curves ($N = 15$, $h^* = 0.2418$).

In Figure 2, the shear-rate-dependent orientation resistance is displayed for $N = 15$ beads ($h^* = 0.2418$). The increase at low shear rates β is confirmed experimentally by light scattering[8,9] and by flow birefringence.[1] The zero-shear-rate limit of the shear-rate-dependent calculation ($N = 15$) leads to a slightly smaller value than the extrapolated ($N \to \infty$) zero-shear-rate orientation resistance (Figure 2). This deviation strongly depends on h^*. It can be kept small by choosing $h^* = 0.2418$ for the shear-rate-dependent ($N = 15$) calculation. We note that for $h^* = 0.396$, which is supposed to be beyond the reasonable range for h^*, the extrapolated orientation resistances (Table 1) are obtained.

3.3. First-Order Perturbation Theory. Another way for attacking the nonlinear effect of hydrodynamic interaction is perturbation theory[15] in the strength of the hydrodynamic interaction parameter $h = (N-1)^{1/2}h^*$. The idea is to write the distribution function as $\psi = \psi_R + \psi_h$, where ψ_R denotes the Rouse distribution function and ψ_h the first-order correction. By using the zero-order (Rouse) result for the second moments $\langle \mathbf{Q}_j \mathbf{Q}_k \rangle_R$, the time evolution equations for the second moments are then expanded up to first order.[15] Unfortunately, this calculation, which has to be performed near four dimensions, leads to divergences of physical quantities such as viscosity or the first normal stress difference that are removed by a renormalization procedure. Finally, there exists a method for refining the first-order perturbation theory by adding higher order contributions. The addition of higher order terms is governed by the renormalization group requirement[15,30] that physically meaningful results should exhibit a power law dependence on the chain length N. The first-order perturbation theory results alone do not fulfil this condition. Adding higher order terms by an exponentiation procedure, however, leads to power law type results. It is important to note that the components D_{12} and $(D_{11} - D_{22})$ of the diffusion tensor do not contain a zero-order contribution, so they cannot be exponentiated. Therefore, the perturbation theory results for the stress tensor $\boldsymbol{\tau}$ and the gyration tensor $\mathbf{G}$ following from exponentiated perturbation theory calculations cannot be compared directly with the result for the diffusion tensor $\mathbf{D}$ in Table 1.

Moreover, we note that in first-order perturbation theory in the hydrodynamic interaction no explicit excluded volume contribution occurs in the expression for the diffusion tensor.[31,32] The fixed-point value of the hydrodynamic interaction parameter characterizing the long-chain behavior, however, changes, when excluded volume effects are included. To that extent, the excluded volume effect on the diffusion tensor may not be neglected. On the other hand, we are interested only in the ratio of anisotropic contributions to the diffusion tensor which do not depend on the mentioned fixed point. Therefore, we can say that the orientation resistance calculated from the diffusion tensor in first-order perturbation theory is not altered by the excluded volume effect.

Comparing the values for the orientation resistance displayed in Table 1, we notice that flow birefringence (stress tensor) leads to larger values than light scattering (gyration tensor) or translational diffusion (diffusion tensor). This observation is compatible with the picture that more local effects are less affected by flow; i.e., the molecular anisotropy at a local scale of the chain is lower than the anisotropy on the scale given by the radius of gyration. In section 2, we mentioned that this picture has been confirmed experimentally by neutron scattering on polymer melts.

The Gaussian approximation is considered as the best of the above-mentioned approximations. The exact agreement of the orientation resistance calculated from the gyration and the diffusion tensor in this approximation is a remarkable feature. However, it is not surprising that these values are not the same in the framework of perturbation theory, since the result for the diffusion tensor cannot be compared directly to the other values, as we already mentioned above.

Recently, Knudsen et al.[33] calculated the reduced steady-state compliance (see section 2) by means of a Brownian dynamics simulation. The corresponding value for the orientation resistance is $m_\tau = 3.4 \pm 0.2$, in good agreement with the Gaussian approximation and perturbation theory. However, this result was obtained only for chains containing less than 20 beads ($N \leq 20$, $h^* = 0.25$[34]), whereas our results are valid for infinitely long chains ($N \to \infty$). If we restrict our calculation to $N = 20$ beads and choose $h^* = 0.25$, the Gaussian approximation leads to $m_\tau = 3.24$, being slightly lower than the value quoted in ref 33.

4. Polydispersity

From experimental flow birefringence investigations,[1-3] it becomes obvious that extremely sharp polymer fractions are needed for a comparison to theoretical results for the orientation resistance. An insufficient sharpness of the investigated fractions is the reason for the low values quoted in the literature (see, for example, Table 6 of ref 2). Cottrell et al.[7] found in light scattering experiments that polydispersity also lowers the m_G^0 values. We therefore want to present the polydispersity correction for the orientation resistance in the case of flow birefringence and light scattering experiments.

Since eqs 2 and 12 can also be used for polydisperse systems, we have the possibility of investigating the effect of polydispersity on the orientation resistance by properly averaging the components of the corresponding tensors with a molecular weight distribution function. In a second step we show how the averaged quantities can be reduced to the properties of monodisperse systems in the limit of small shear rates and finally we evaluate them for two specific distribution functions.

4.1. Averaging of the Stress and the Gyration Tensor. Assuming that the individual molecular contributions to the stress are additive, the polydispersity of the polymer solution is reflected in the number-average (denoted by $\langle\langle ... \rangle\rangle_n$) stress tensor, i.e.

$$\frac{\langle\langle \tau_{11} - \tau_{22} \rangle\rangle_n}{2\langle\langle \tau_{12} \rangle\rangle_n} = \frac{1}{2} \frac{\int_0^\infty dM\, \varrho_n(M)[\tau_{11}(M) - \tau_{22}(M)]}{\int_0^\infty dM\, \varrho_n(M)\tau_{12}(M)} \tag{18}$$

where $\varrho_n(M)dM$ is proportional to the number of polymer molecules with molecular weight between M and $M + dM$. The normalization condition is $\int dM\, \varrho_n(M) = 1$.

In the case of light scattering, we further assume that the total intensity scattered from a polydisperse system is the sum of contributions of the individual molecules. Then it can be shown[18] that the experimentally accessible Rayleigh ratio for a polydisperse system depends on the z average of the form factor $P(\mathbf{q})$. This leads to the following expression:

$$\frac{\langle\langle G_{11} - G_{22} \rangle\rangle_z}{2\langle\langle G_{12} \rangle\rangle_z} = \frac{1}{2} \frac{\int_0^\infty dM\, \varrho_n(M)M^2[G_{11}(M) - G_{22}(M)]}{\int_0^\infty dM\, \varrho_n(M)M^2 G_{12}(M)} \tag{19}$$

In these equations we introduced the number- and the weight-average molecular weights M_n and M_w, respectively,

$$M_n := \int dM\, \varrho_n(M)M \tag{20}$$

$$M_w := \frac{\int dM\, \varrho_n(M)M^2}{\int dM\, \varrho_n(M)M} \tag{21}$$

4.2. Reduction to Monodisperse Quantities by Scaling Arguments. On a scale that is large compared to the size of the monomers, the macromolecules are found to be self-similar; i.e., the coil structure is the same on different local scales. In static polymeric systems, self-similarity leads to scaling laws such as $(R_G^2)^{1/2} \sim M^\nu$, with $\nu = 1/2$ for a pure random walk chain and $\nu \simeq 3/5$ for a random walk chain including excluded volume (see, e.g., ref 35).

We now consider the scaling form of the stress and the gyration tensor in a nonequilibrium solution. For sufficiently long chains, we can write

$$\boldsymbol{\tau} = -n_p k_B T \mathbf{f}^\tau(\beta) \tag{22}$$

$$\mathbf{G} = a^2 N^{2\nu} \mathbf{f}^G(\beta) \tag{23}$$

where a is a local length scale, independent of $\dot\gamma$ and N. The exponent 2ν follows from $\langle R_G^2 \rangle \sim N^{2\nu}$ at equilibrium. The dimensionless functions $\mathbf{f}^\tau$ and $\mathbf{f}^G$ depend on the dimensionless reduced shear rate β, which is the product of the characteristic time scale $\tilde\lambda = [\eta]_0 \eta_s M/RT$ and the shear rate $\dot\gamma$ (see eq 3). We note that the chain length dependence of $\mathbf{f}^\tau$ and $\mathbf{f}^G$ is confined to the molecular weight dependence of β:

$$\beta \sim N^b \dot\gamma \tag{24}$$

The values for b can be found in Table 2. For example,

Table 2. Exponents ν and b for the Free-Draining Case (Rouse), Hydrodynamic Interaction Only (HI), and Hydrodynamic Interaction and Excluded Volume (HI,EV)

	Rouse	HI	HI,EV
ν	1/2	1/2	0.588(1)
b	2	3/2	1.764(3)

when keeping β at a constant value and increasing $\dot{\gamma}$, the corresponding shorter chain length means that the polymers are affected on a smaller scale at higher shear rates.

At least for the Rouse model, or models including hydrodynamic interaction, eqs 22 and 23 can be checked explicitly and they seem natural also after inclusion of excluded volume. The values of the exponents ν and b depend on the intramolecular interactions that are taken into account. For the Rouse model $b = 2$,[10] for models that include hydrodynamic interaction $b = 1.5$,[15,28] and for models with hydrodynamic interaction and excluded volume $b = 3\nu$ with $\nu \simeq 0.588$, i.e., $b \simeq 1.764$ (see also Table 2).

Equations 22 and 23 suggest that if the stress and the gyration tensor components are plotted against β and are properly normalized, the curves for different molecular weights should all lie on a single curve (for experiments, see, e.g., ref 36).

For small shear rates it follows from eq 22 that for fixed $\dot{\gamma}$

$$\tau_{12} \sim M^b \qquad (n \text{ fixed}) \tag{25}$$

$$(\tau_{11} - \tau_{22}) \sim M^{2b} \qquad (n \text{ fixed}) \tag{26}$$

and from eq 23 that

$$G_{12} \sim M^{b+2\nu} \tag{27}$$

$$(G_{12} - G_{22}) \sim M^{2(b+\nu)} \tag{28}$$

Let us turn to flow birefringence first. Equations 25 and 26 lead to

$$\frac{\langle\langle \tau_{11} - \tau_{22}\rangle\rangle_n}{2\langle\langle \tau_{12}\rangle\rangle_n} = \frac{1}{2}\frac{\psi_1(M_0,\dot{\gamma}=0)}{\eta_p(M_0,\dot{\gamma}=0)}\frac{1}{M_0{}^b}\frac{\langle\langle M^{2b}\rangle\rangle_n}{\langle\langle M^b\rangle\rangle_n}\dot{\gamma} \tag{29}$$

The expression $\eta_p(M_0,\dot{\gamma}=0)$ denotes the polymer contribution to the zero-shear-rate viscosity evaluated at a fixed chain length corresponding to a reference molecular weight M_0, and $\psi_1(M_0,\dot{\gamma}=0)$ has an analogous meaning. The reference value M_0 could arbitrarily be chosen as $M_0 = M_n$, where M_n means the number-average molecular mass. We define the number-average reduced shear rate β_n by

$$\beta_n := \frac{\eta_p(M_0,\dot{\gamma}=0)}{n_p k_B T}\int \mathrm{d}M\, \varrho_n(M)\left(\frac{M}{M_0}\right)^b \dot{\gamma} \tag{30}$$

$$= \frac{[\eta]_0 \eta_s}{RT} M_n \dot{\gamma} \qquad (\text{for } n_p \to 0) \tag{31}$$

so that eq 29 becomes

$$\frac{\langle\langle \tau_{11} - \tau_{22}\rangle\rangle_n}{2\langle\langle \tau_{12}\rangle\rangle_n} = \frac{\beta_n}{m_\tau^0 p_\tau} \tag{32}$$

where m_τ^0 is the orientation resistance for a monodisperse system and the polydispersity factor p_τ is given by

$$p_\tau = \frac{\langle\langle M^b\rangle\rangle_n{}^2}{\langle\langle M^{2b}\rangle\rangle_n} \tag{33}$$

We emphasize that the result in eq 32 does not depend on the value of the reference molecular weight M_0. If we introduce the following molecular weight averages[10]

$$M_{z+j} = \frac{\langle\langle M^{3+j}\rangle\rangle_n}{\langle\langle M^{2+j}\rangle\rangle_n} \tag{34}$$

we can express p_τ in a different way. For $j = -2$, -1, and 0 the quantities M_{z+j} are called respectively the number-average molecular weight M_n, the weight-average molecular weight M_w, and the z-average molecular weight M_z. For the free-draining case (Rouse model, $b = 2$) p_τ can be written as

$$p_\tau = \frac{M_w M_n}{M_{z+1} M_z} \tag{35}$$

For small shear rates we have for the orientation angle of a polydisperse system

$$\chi_\tau = \frac{\pi}{4} - \frac{1}{2}\frac{1}{m_\tau^0 p_\tau}\beta_n \tag{36}$$

so that by plotting the orientation angle χ_τ against the number-average reduced shear rate β_n, the experimental value for the polydisperse orientation resistance $m_\tau^0 p_\tau$ is obtained from the initial slope of the curve. This value can then, for example, be compared to the theoretical value m_τ^0 or it can be compared to other measurements with the help of the polydispersity factor p_τ. From eq 32 it follows directly how systems with different polydispersities can be compared:

$$m_\tau^0(p_\tau(1)) = \frac{p_\tau(1)}{p_\tau(2)} m_\tau^0(p_\tau(2)) \tag{37}$$

If the orientation resistance $m_\tau^0(p_\tau(1))$ of system (1) and $p_\tau(1)$ are known, then the polydispersity factor $p_\tau(2)$ for system (2) can be predicted from (37) after a measurement of the orientation resistance $m_\tau^0(p_\tau(2))$.

The influence of polydispersity upon flow birefringence in dilute polymer solutions was already discussed in refs 1 and 3 in the context of the reduced steady-state compliance. The correction factor p occurring in these papers coincides with the inverse of p_τ.

The same procedure applies to the gyration tensor, which determines light scattering experiments performed in the Guinier regime. With the help of (27) and (28) we can write down the ratio (19) at small shear rates using again the reduced shear rate β_n (30) as follows:

$$\frac{\langle\langle G_{11} - G_{22}\rangle\rangle_z}{2\langle\langle G_{12}\rangle\rangle_z} = \frac{\beta_n}{m_G^0 p_G} \tag{38}$$

with the polydispersity factor

$$p_G = \frac{\langle\langle M^b\rangle\rangle_n \langle\langle M^{b+2\nu+2}\rangle\rangle_n}{\langle\langle M^{2b+2\nu+2}\rangle\rangle_n} \tag{39}$$

By repeating the arguments used for flow birefringence, the orientation angle of a polydisperse system determined by light scattering at small shear rates becomes

$$\chi_G = \frac{\pi}{4} - \frac{1}{2}\frac{1}{m_G^0 p_G}\beta_n \tag{40}$$

We would like to emphasize that eq 40 can also be employed for neutron scattering experiments as long as the validity of the Guinier regime (see eq 8) is guaranteed.

Finally, we can write down an equation that allows for a comparison of systems with different polydispersities analogously to eq 37 for flow birefringence

$$m_G^0(p_G(1)) = \frac{p_G(1)}{p_G(2)} m_G^0(p_G(2)) \tag{41}$$

In expression 31 for the reduced shear rate β_n, sometimes the number-average molecular weight M_n is replaced by the weight-average molecular weight M_w. The reduced shear rate is then denoted by β_w. Formulas (36) and (37) and (40) and (41) can still be used with β_n replaced by β_w. However, the polydispersity factors then have to be multiplied by a factor $w = M_w/M_n$.

4.3. Polydispersity Factors for the Schulz–Zimm and the Logarithmic-Normal Distribution Functions. One of the most successful examples for distribution functions derived on a kinetic basis of the polymerization process is the two-parameter Schulz–Zimm distribution function[37,38]

$$\varrho_n(M)\,dM = \frac{(y+1)^{y+1}}{\Gamma(y+1)}\frac{M^y}{M_n^{y+1}}\exp\left[-\frac{M}{M_n}(y+1)\right]dM \tag{42}$$

$$y = \frac{M_n^2}{\langle\langle M^2\rangle\rangle_n - M_n^2} - 1 = \frac{w-2}{1-w} \tag{43}$$

$$w = M_w/M_n \tag{44}$$

where $\varrho_n(M)\,dM$ is the number fraction of molecules with molecular weights between M and $M + dM$. The Schulz–Zimm distribution applies, e.g., to the free-radical chain polymerization[37] or to the kinetics of the stepwise addition and condensation polymerization.[39]

An example of an empirical distribution function is the logarithmic-normal distribution:[40,41]

$$\varrho_n(M)\,dM = \frac{1}{\pi^{1/2}(2\ln w)^{1/2}}\frac{M_n}{M^2}\exp\left[-\frac{1}{2\ln w}\times \ln^2\left(\frac{M}{M_n w^{1/2}}\right)\right]dM \tag{45}$$

The molecular weight distribution functions (42) and (45) lead to polydispersity factors p_τ and p_G displayed in Table 3. They are evaluated for different discrete values of the polydispersity in Table 4. In Figures 3 (Θ solvent) and 4 (good solvent) we display the inverse polydispersity factors as continuous functions of the polydispersity w. First, we can see that the polydispersity factors p_τ and p_G involved in the measurement of the intrinsic orientation resistance m^0 are very sensitive to polydispersity and further allow for a clear distinction between the Schulz–Zimm and the logarithmic-normal distribution. The effect is more pronounced in the case of light scattering than in the case of flow birefringence. Second, it can be inferred that excluded volume increases the polydispersity effect.

Finally, we note that in principle the polydispersity factors p_τ and p_G can also be calculated for other distribution functions. We mention the Poisson distribution[39] and the generalized exponential distribution.[42–44] Moreover, upon mixing two weight fractions of polymeric systems described by one of the above-mentioned distribution functions, bimodal distributions can be obtained. Even for such systems the polydispersity factors p_τ and p_G can be calculated.

Table 3. Polydispersity Factors for the Schulz–Zimm and the Logarithmic-Normal Distribution as Functions of $y = (w-2)/(1-w)$, Where w Denotes the Polydispersity (ν and b are displayed in Table 2)

distribution	p_τ	p_G
Schulz–Zimm	$\frac{\Gamma^2(y+b+1)}{\Gamma(y+1)\Gamma(y+2b+1)}$	$\frac{\Gamma(y+b+1)\Gamma(y+b+2\nu+3)}{\Gamma(y+1)\Gamma(y+2b+2\nu+3)}$
logarithmic-normal	w^{-b^2}	$w^{-(b^2+2\nu b+2b)}$

Table 4. Polydispersity Factors for the Schulz–Zimm and the Logarithmic-Normal Distribution[a]

	Schulz–Zimm distribution				log-normal distribution			
	p_τ		p_G		p_τ		p_G	
w	HI	HI,EV	HI	HI,EV	HI	HI,EV	HI	HI,EV
1.00	1.000	1.000	1.000	1.000	1.000	1.000	1.000	1.000
1.05	0.898	0.864	0.740	0.682	0.896	0.859	0.719	0.654
1.10	0.815	0.758	0.579	0.503	0.807	0.743	0.526	0.436
1.15	0.745	0.674	0.471	0.391	0.730	0.647	0.389	0.296
1.20	0.685	0.605	0.394	0.316	0.664	0.567	0.292	0.204
1.25	0.634	0.548	0.337	0.262	0.605	0.499	0.222	0.143
1.30	0.590	0.501	0.294	0.223	0.554	0.442	0.170	0.102
1.35	0.551	0.460	0.259	0.193	0.509	0.393	0.132	0.073
1.40	0.517	0.426	0.232	0.169	0.469	0.351	0.103	0.053
1.45	0.487	0.396	0.209	0.150	0.433	0.315	0.081	0.039
1.50	0.460	0.369	0.190	0.135	0.402	0.283	0.065	0.029
1.55	0.436	0.346	0.174	0.122	0.373	0.256	0.052	0.022
1.60	0.414	0.325	0.160	0.111	0.347	0.232	0.042	0.017
1.65	0.394	0.307	0.148	0.102	0.324	0.210	0.034	0.013
1.70	0.376	0.291	0.138	0.094	0.303	0.192	0.028	0.010
1.75	0.360	0.276	0.129	0.087	0.284	0.175	0.023	0.008
1.80	0.344	0.262	0.121	0.081	0.266	0.161	0.019	0.006
1.85	0.330	0.250	0.114	0.076	0.251	0.147	0.016	0.005
1.90	0.318	0.239	0.108	0.071	0.236	0.136	0.013	0.004
1.95	0.306	0.228	0.102	0.067	0.223	0.125	0.011	0.003
2.00	0.295	0.219	0.097	0.063	0.210	0.116	0.009	0.002
2.10	0.275	0.202	0.088	0.057	0.188	0.099	0.007	0.002
2.20	0.257	0.188	0.080	0.051	0.170	0.086	0.005	0.001
2.30	0.242	0.175	0.074	0.047	0.154	0.075	0.004	0.001
2.40	0.228	0.164	0.068	0.043	0.139	0.066	0.003	0.000
2.50	0.216	0.154	0.064	0.040	0.127	0.058	0.002	0.000
2.60	0.205	0.145	0.059	0.037	0.116	0.051	0.002	0.000
2.70	0.195	0.138	0.056	0.035	0.107	0.045	0.001	0.000
2.80	0.186	0.131	0.053	0.033	0.099	0.041	0.001	0.000
2.90	0.177	0.124	0.050	0.031	0.091	0.036	0.001	0.000
3.00	0.170	0.118	0.047	0.029	0.084	0.033	0.001	0.000
3.50	0.140	0.096	0.037	0.023	0.060	0.020	0.000	0.000
4.00	0.119	0.081	0.031	0.018	0.044	0.013	0.000	0.000
4.50	0.103	0.070	0.026	0.016	0.034	0.009	0.000	0.000
5.00	0.091	0.061	0.023	0.013	0.027	0.007	0.000	0.000
6.00	0.074	0.049	0.018	0.011	0.018	0.004	0.000	0.000
7.00	0.064	0.041	0.015	0.009	0.013	0.002	0.000	0.000
8.00	0.053	0.035	0.013	0.007	0.009	0.002	0.000	0.000
9.00	0.046	0.031	0.011	0.006	0.007	0.001	0.000	0.000
10.00	0.042	0.027	0.010	0.006	0.006	0.001	0.000	0.000

[a] HI, hydrodynamic interaction only (Θ solvent); HI,EV, hydrodynamic interaction and excluded volume (good solvents).

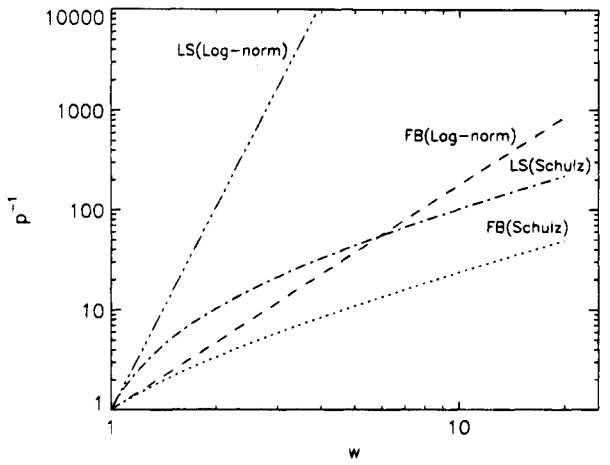

Figure 3. Inverse polydispersity factor for light scattering (LS) and flow birefringence (FB) in a Θ solvent evaluated for the Schulz–Zimm (Schulz) and the logarithmic-normal (Log-norm) distribution function.

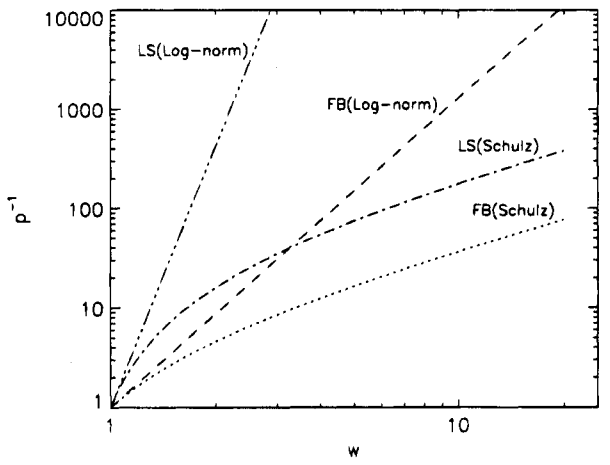

Figure 4. Inverse polydispersity factor for light scattering (LS) and flow birefringence (FB) in a good solvent evaluated for the Schulz–Zimm (Schulz) and the logarithmic-normal (Log-normal) distribution function.

4.4. A Comparison to Experimental Data. Once a precise gauge measurement of the orientation resistance $m^0(p(1))$ on a dilute polymer solution (system (1)) with known polydispersity factor $p(1)$ has been performed, eqs 37 and 41 allow for a determination of the polydispersity factor $p(2)$ of a polydisperse system (2). For this purpose, the orientation resistance $m^0(p(2))$ has to be measured. If the type of molecular mass distribution of system (2) is known, e.g., from the kinetics of the polymerization process, then the polydispersity factor directly yields the polydispersity w. In Table 4 we display the conversion of the polydispersity factor p to the polydispersity w for the Schulz–Zimm and the logarithmic-normal distribution.

Alternatively, one can think of combining light scattering and flow birefringence measurements in order to determine the type of the molecular mass distribution as well as the polydispersity w with the help of Figures 3 and 4.

For a first comparison to experimental flow birefringence data, we take a measurement of (1) Janeschitz-Kriegl et al.[4] and another experiment (2) of the same author.[5] In both (1) and (2) linear polystyrene samples in a good solvent with polydispersities $w = 1.52$ and $w \leq 1.09$, respectively, were used. The first sample was polymerized by a free-radical polymerization. From a kinetic point of view, the molar mass of sample 1 should then be distributed according to the Schulz–Zimm distribution. Indeed this sample yields practically the theoretical value 1.5 for a linear polymer system with chain growth termination by combination. Though system 2 was polymerized by an anionic polymerization process which should yield Poisson-distributed weight fractions, system 2 seems to fit the Schulz–Zimm distribution as well.[3] The orientation resistances that we obtain from these measurements are (1) $m_\tau^0(p_\tau) = 1.43$ with $w = 1.52$ and (2) $m_\tau^0(p_\tau) = 2.70$ with $w = 1.09$. We can take experiment 1 as a reference measurement and try to predict the polydispersity of system 2 with the help of eq 37. By doing so, we obtain $w = 1.14$. This value is in good agreement with the quoted value $w = 1.09$.

Experiments 1 and 2 were both performed in good solvents. Nevertheless we can try to compare them to the theoretical values of Table 1, which are valid only for Θ solvents. In both cases the values lie around $m_\tau^0 = 3.5$. This is in good agreement with the theoretical value calculated by means of the Gaussian approximation. However, we expect from the discussion in section 3 that the orientation resistance in Θ solvents is somewhat higher than in good solvents. This is confirmed by an experiment of Daum[3] on very sharply distributed linear polystyrene in a Θ solvent. The obtained value is $m_\tau^0 = 4.34$, which lies between the Zimm value and the value of the Gaussian approximation (see Table 1).

Only a few light scattering experiments have been performed on dilute polymer solutions undergoing shear flow. In recent publications[8] high molar mass polystyrene has been investigated in Θ as well as in good solvents. The molecular weight distribution was of a Schulz–Zimm type. Unfortunately, the polydispersity range of the samples employed in ref 8 is very small so that formula (41) cannot be applied. However, it has been observed by Cottrell et al.[7] that polydispersity lowers the value of the orientation resistance. This is in accordance with our results.

From ref 8 we can take the sample with a polydispersity degree $w \leq 1.20$. The quoted orientation resistance value in a Θ solvent is $m^0(p_G) = 2.23$. Since the data were plotted against β_w instead of β_n, the polydispersity factor p_G has to be multiplied by a factor $w \leq 1.20$, leading to $m_G^0 \leq 4.72$. Obviously, this value is higher than the values predicted by theory. It is much closer to the theoretical values for flow birefringence than to the ones for light scattering. Further measurements will be necessary to decide whether there are significant deviations from the theoretical values.

5. Concluding Remarks

We have discussed the different origins of flow birefringence and light scattering for dilute polymer solutions undergoing shear flow by deriving the equations that relate the orientation angle to the stress and the gyration tensor, respectively. It is convenient to describe the orientational behavior with the help of the orientation resistance m, which can be obtained by diagonalizing the corresponding tensorial quantity.

The orientation resistance m has been calculated in the framework of bead–spring models using different approximation schemes. The Rouse and the Zimm model lead to constant values for the orientation resistance in both cases, flow birefringence and light scattering. We found that the original Zimm value ($m_\tau^0 =$

4.88) must be corrected to $m_\tau^0 = 4.83$. In the Rouse, as well as in the Zimm, model, the diffusion tensor is isotropic. Therefore, the orientational behavior arising from the diffusional properties of the flowing polymer solution cannot be discussed in these models. The Gaussian approximation, on the other hand, predicts the smallest value of the orientation resistance for the diffusion and the gyration tensor (light scattering) and the largest for the stress tensor (flow birefringence). The following picture may help to understand these results: The polymer coil can be oriented on different scales. If the orientation takes place on a very local scale (stress tensor), the effect should be less pronounced than if the orientation is a global one (diffusion and gyration tensor).

Further we showed that the Gaussian approximation leads to a shear-rate-dependent orientation resistance as expected from flow birefringence and light scattering experiments.

We have quantitatively investigated the polydispersity effect for both measurement techniques. From this, it can be inferred that polydispersity has a stronger effect on the orientation resistance measured by light scattering than by flow birefringence, though it lowers the values in both cases.

The comparison to experiments shows that our theoretical investigations of the polydispersity effect describes the situation of flow birefringence experiments very well. Indeed, the agreement with experiments is so good that one could think of using flow birefringence measurements to determine the polydispersity of linear polymer samples in dilute solution once a precise gauge measurement has been performed. This was illustrated with the help of two independent measurements on linear polystyrene in good solvents.

If one wishes to obtain the full molecular weight distribution rather than only the polydispersity w, one needs to measure a function rather than only a single value of the orientation resistance. For example, one can measure the orientation resistance as a function of the shear rate $\dot{\gamma}$. Since, with increasing shear rate, faster processes are activated, increasingly shorter molecules contribute to the orientation resistance. It should therefore be possible to reconstruct the molecular weight distribution from the shear-rate-dependent orientation resistance. The experimental verification of this idea for mixtures of narrowly distributed polymers is planned in our research group. One could analyze the time-dependent orientation resistance in start-up or cessation of steady shear flow in a similar spirit.

In the case of light scattering, the success of such a procedure is unclear because, to the best of our knowledge, the available experiments were performed on systems with a small polydispersity range.

Polymer characterization techniques have been developed intensively during the past 20 years. Therefore, further measurements on systems with well-characterized molecular weight distributions should be performed in order to obtain a precise gauge measurement and to test the polydispersity predictions.

Acknowledgment. The authors thank the Swiss National Foundation for Scientific Research (Grant No. 20-36073.92) for financial support. Generous allocations of CPU time of the Swiss Federal Institute of Technology on the Cray Y-MP supercomputer are gratefully acknowledged.

References and Notes

(1) Janeschitz-Kriegl, H. *Adv. Polym. Sci.* **1969**, *6*, 170.
(2) Tsvetkov, V. N. *Sov. Phys. Usp.* **1964**, *6* (5), 639.
(3) Daum, U. *J. Polym. Sci., Part A-2* **1968**, *6*, 141.
(4) Janeschitz-Kriegl, H.; Henrici-Olivé, G.; Olivé, S. *Kolloid Z. Z. Polym.* **1963**, *191* (2), 97.
(5) Janeschitz-Kriegl, H. *Kolloid Z. Z. Polym.* **1965**, *203* (2), 119.
(6) Hongladarom, K.; Burghardt, W. R.; Baek, S.-G.; Cementwala, S.; Magda, J. J. *Macromolecules* **1993**, *26*, 772.
(7) Cottrell, F. R.; Merrill, E. W.; Smith, K. A. *J. Polym. Sci., Part A-2* **1969**, *7*, 1415.
(8) Zisenis, M. *Streulichtmessungen zum Studium der Orientierung von Hoch-Polymeren durch Scherströmung*, Wissenschaftliche Schriftenreihe Chemie Bd 13; Dr. Köster: Berlin, 1994.
(9) Link, A.; Springer, J. *Macromolecules* **1993**, *26*, 464.
(10) Bird, R. B.; Curtiss, C. F.; Armstrong, R. C.; Hassager, O. *Dynamics of Polymeric Liquids. Kinetic Theory*, 2nd ed.; Wiley-Interscience: New York, 1987; Vol. 2.
(11) Rouse, P. E. *J. Chem. Phys.* **1953**, *21*, 1272.
(12) Zimm, B. H. *J. Chem. Phys.* **1956**, *24*, 269. A corrected version of that paper can be found in: Hermans, J. J. *Polymer Solutions Properties, Part II: Hydrodynamics and Light Scattering*; Dowden, Hutchinson and Ross: Stroudsburg, PA, 1978; pp 73–84. For corrections to Zimm's paper, see also: Williams, M. C. *J. Chem. Phys.* **1965**, *42*, 2988; **1965**, *43*, 4542.
(13) Öttinger, H. C. *J. Chem. Phys.* **1989**, *90* (1), 463.
(14) Wedgewood, L. E. *J. Non-Newtonian Fluid Mech.* **1989**, *31*, 127.
(15) Öttinger, H. C.; Rabin, Y. *J. Non-Newtonian Fluid Mech.* **1989**, *33*, 53.
(16) Tschoegl, N. W. *J. Chem. Phys.* **1966**, *44* (12), 4615.
(17) Schmitz, K. S. *An Introduction to Dynamic Light Scattering by Macromolecules*; Academic Press: Boston, 1990.
(18) Kratochvil, P. In *Light Scattering from Polymer Solutions*; Huglin, M. B., Ed.; Academic Press: London, 1972; pp 333–384.
(19) Carl, W. Modellrechnungen an Polymerlösungen im Schergefälle, Ph.D. Thesis, TU Berlin, 1992.
(20) Peterlin, A.; Heller, W.; Nakagaki, M. *J. Chem. Phys.* **1958**, *28* (3), 470.
(21) Peterlin, A. *J. Polym. Sci.* **1957**, *23*, 189.
(22) Kröger, M.; Loose, W.; Hess, S. *J. Rheol.* **1993**, *37* (6), 1057.
(23) Muller, R.; Picot, C. *Makromol. Chem., Macromol. Symp.* **1992**, *56*, 107.
(24) Muller, R.; Pesce, J. J.; Picot, C. *Macromolecules* **1993**, *26*, 4356.
(25) Öttinger, H. C. *Phys. Rev. A* **1989**, *40* (5), 2664.
(26) Daum, U., unpublished work.
(27) Osaki, K.; Schrag, J. L.; Ferry, J. D. *Macromolecules* **1972**, *5* (2), 144.
(28) Öttinger, H. C. *J. Chem. Phys.* **1987**, *86* (6), 3731.
(29) Zimm, B. H.; Roe, G. M.; Epstein, L. F. *J. Chem. Phys.* **1956**, *24* (2), 279.
(30) Oono, Y. In *Advances in Chemical Physics*; Prigogine, I., Rice, S. A., Eds.; Wiley: New York, 1985; Vol. LXI, pp 301–437.
(31) Öttinger, H. C. *Phys. Rev. A* **1990**, *41* (8), 4413.
(32) Zylka, W.; Öttinger, H. C. *Macromolecules* **1991**, *24*, 484.
(33) Knudsen, K. D.; Elgsaeter, A.; López Cascales, J. J.; Garcia de la Torre, J. *Macromolecules* **1993**, *26*, 3851.
(34) Knudsen, K. D., personal communication.
(35) de Gennes, P.-G. *Scaling Concepts in Polymer Physics*; Cornell University Press: Ithaca, NY, 1991.
(36) Graessley, W. W. *Adv. Polym. Sci.* **1974**, *16*, 1.
(37) Schulz, G. V. *Z. Phys. Chem.* **1939**, *B43*, 25.
(38) Zimm, B. H. *J. Chem. Phys.* **1948**, *16* (12), 1099.
(39) Flory, P. J. *Principles of Polymer Chemistry*; Cornell University Press: Ithaca, NY, 1953.
(40) Lansing, W. D.; Kraemer, E. O. *J. Am. Chem. Soc.* **1935**, *57*, 1369.
(41) Wesslau, H. *Makromol. Chem.* **1956**, *20*, 111.
(42) Muus, L. T.; Stockmayer, W. H. In *Textbook of Polymer Chemistry*; Billmayer, F. W., Jr., Ed.; Interscience: New York, London, 1962.
(43) Tung, L. H. *J. Polym. Sci.* **1956**, *20*, 495.
(44) Weibull, W. *J. Appl. Mech.* **1951**, *18*, 293.

MA950309G